Available online at www.sciencedirect.com

ScienceDirect

www.elsevier.com/locate/jes

JES JOURNAL OF ENVIRONMENTAL SCIENCES

www.jesc.ac.cn

Interaction of polyhydroxy fullerenes with ferrihydrite: adsorption and aggregation

Jing Liu[1,2], *Runliang Zhu*[1,*], *Tianyuan Xu*[1,2], *Mingwang Laipan*[1,2], *Yanping Zhu*[1,2], *Qing Zhou*[1,2], *Jianxi Zhu*[1], *Hongping He*[1,2]

1. *Key Laboratory of Mineralogy and Metallogeny, Guangzhou Institute of Geochemistry, Chinese Academy of Sciences, Guangdong Provincial Key Laboratory of Mineral Physics and Material Research & Development, Guangzhou 510640, China*
2. *University of Chinese Academy of Sciences, Beijing 100049, China*

ARTICLE INFO

Article history:
Received 6 April 2017
Revised 13 June 2017
Accepted 13 June 2017
Available online 24 June 2017

Keywords:
Nanoparticles
Polyhydroxy fullerenes
Ferrihydrite
Adsorption
Aggregation

ABSTRACT

The rapid development of nanoscience and nanotechnology, with thousands types of nanomaterials being produced, will lead to various environmental impacts. Thus, understanding the behaviors and fate of these nanomaterials is essential. This study focused on the interaction between polyhydroxy fullerenes (PHF) and ferrihydrite (Fh), a widespread iron (oxyhydr)oxide nanomineral and geosorbent. Our results showed that PHF were effectively adsorbed by Fh. The adsorption isotherm fitted the D-R model well, with an adsorption capacity of 67.1 mg/g. The adsorption mean free energy of 10.72 kJ/mol suggested that PHF were chemisorbed on Fh. An increase in the solution pH and a decrease of the Fh surface zeta potential were observed after the adsorption of PHF on Fh; moreover, increasing initial solution pH led to a reduction of adsorption. The Fourier transform infrared spectra detected a red shift of C–O stretching from 1075 to 1062 cm^{-1} and a decrease of Fe–O bending, implying the interaction between PHF oxygenic functional groups and Fh surface hydroxyls. On the other hand, PHF affected the aggregation and reactivity of Fh by changing its surface physicochemical properties. Aggregation of PHF and Fh with individual particle sizes increasing from 2 nm to larger than 5 nm was measured by atomic force microscopy. The uniform distribution of C and Fe suggested that the aggregates of Fh were possibly bridged by PHF. Our results indicated that the interaction between PHF and Fh could evidently influence the migration of PHF, as well as the aggregation and reactivity of Fh.

Introduction

The environmental behaviors and fate of engineered nanoparticles have raised widespread concerns nowadays (Nowack et al., 2012; Hou et al., 2017). Among these engineered nanoparticles, fullerenes and their derivatives have gained great attention due to their potential applications in a variety of areas, including medicine, hydrogen storage, catalysis, solar cells, *etc.* (Kratschmer et al., 1990; Zhang et al., 2016) Industrial-scale production of fullerenes and their derivatives has reached tons per year (Murayama et al., 2004), and a large increase is expected in the near future. At the same time, most of these products will eventually end up entering into the environment as a consequence of both natural processes and human activities. Polyhydroxy fullerenes (PHF, *i.e.*, fullerenols), the hydroxylated derivatives of fullerenes, are significantly more soluble in aqueous environments (ranging from 1×10^{-3} to 5×10^{-3} mol/L), depending on the number of hydroxyl

* *Corresponding author*. E-mail: zhurl@gig.ac.cn (Runliang Zhu).

http://dx.doi.org/10.1016/j.jes.2017.06.016
1001-0742 © 2017 The Research Center for Eco-Environmental Sciences, Chinese Academy of Sciences. Published by Elsevier B.V.

groups, which varies from 12 to 40 (Zhang et al., 2010; Indeglia et al., 2014), and are more likely to be applied in the aqueous phase. In addition, PHF have been recognized as the primary products of fullerenes in the environment, because many factors such as photo-oxidation (*via* sunlight), exposure to oxidants (*e.g.*, hydroxyl radicals and ozone), and microbes' action can transform fullerenes into PHF (Qu et al., 2012; Indeglia et al., 2013). Moreover, a number of recent studies have shown that PHF could be toxic to some organisms and human cell lines (Yamawaki and Iwai, 2006; Injac et al., 2013). For instance, a dose of $C_{60}(OH)_{24}$ at a concentration of 10–100 μg/mL was demonstrated to induce cytotoxic injury and inhibit the growth of endothelial cells (Yamawaki and Iwai, 2006). In consideration of their wide availability, strong migration ability, and potential toxicity, investigation of the environmental behaviors and fate of PHF is necessary and urgent.

Recently, a series of studies has investigated the environmental behaviors of PHF. For instance, Wang et al. (2016) found that PHF could be accumulated in the vascular cylinder of wheat roots and could promote root elongation and chlorophyll synthesis. Heimann et al. (2015) investigated the reactions of PHF with a wide range of metal salts and observed the formation of insoluble cross-linked polymers. Fortner et al. (2012) investigated the interaction of nC_{60} with clay minerals (*e.g.*, montmorillonite and kaolinite) and a synthetic layered double hydroxide, and suggested that the interaction between nC_{60} and the clay minerals was dominated by electrostatic forces. Chen et al. (2016) discovered that montmorillonite modified with the branched polymer polyethylenimine (PEI) had favorable adsorption capacity toward PHF, which could increase with the loading of PEI. Recently, several studies also focused on the light-induced reactions of PHF, and light-induced production of $^1O_2$ and $O_2^{\cdot-}$ by PHF was reported (Kong et al., 2009). On the other hand, considerably fewer studies concerned the interaction between PHF and soil minerals, especially mineral nanoparticles.

As iron (oxyhydr)oxides are ubiquitous in the environment and contain abundant surface-active groups (*e.g.*, Fe-OH), they are considered to be an important family of geosorbents that can significantly affect the environmental behaviors of various chemicals (*e.g.*, heavy metal cations, oxyanions) (Shi et al., 2009; Tang et al., 2010; Mitsunobu et al., 2013). Among the various types of iron (oxyhydr)oxides, ferrihydrite (Fh), with very large specific surface area and abundant active surface groups, has drawn particular interest as a geosorbent and natural catalyst (Raven et al., 1998; Jambor and Dutrizac, 1998; Wang et al., 2013). Fh can be widely found in waters, sediments, soils, mine wastes, and acid mine drainage (Jambor and Dutrizac, 1998). An ample amount of literature (Swedlund and Webster, 1999; Hiemstra et al., 2009) has suggested that Fh has higher adsorption capacities toward various cations, anions, and organic species than other crystallized iron (oxyhydr)oxides. The interaction of Fh with these species could include ligand exchange, electrostatic interactions, surface precipitation, *etc.* (Swedlund and Webster, 1999; Hiemstra et al., 2009; Wang et al., 2013). In addition, its interactions with environmental constituents could in turn affect its own reactivity and fate (Schwertmann and Murad, 1983; Das et al., 2011).

The objective of this work is to improve the understanding of the interaction between PHF and iron (oxyhydr)oxides, and thus help to predict the environmental behaviors and fate of PHF. Fh was chosen as a representative iron (oxyhydr)oxide. The adsorption behaviors of PHF on Fh as influenced by various factors, as well as the aggregation of the two, were investigated. Our results showed that Fh could strongly adsorb PHF through ligand and anion exchange. Moreover, the loading of PHF had significant influence on the surface physicochemical properties of Fh, and thus could alter the aggregation and reactivity of Fh.

1. Materials and methods

1.1. Chemicals

PHF ($C_{60}(OH)_{21}\cdot 6H_2O$) was purchased from Suzhou Dade Carbon Nanotechnology Co., Ltd. (Suzhou, China); whereas NaOH, HNO_3, $Fe(NO_3)_3\cdot 9H_2O$, $Cd(NO_3)_2\cdot 4H_2O$, NaH_2PO_4, Na_2SO_4, and $NaHCO_3$ of analytical grade (purity > 99%) were obtained from Shanghai Chemical Co., China. All reagents were used as received. All glassware and plasticware were cleaned by soaking overnight in diluted HCl solution and washed in ultra-pure water (ρ > 18 MΩ/cm) before each experiment.

1.2. Ferrihydrite synthesis

Fh was synthesized according to the process reported by Schwertmann and Cornell (1991) with slight modification. Specifically, a solution of $Fe(NO_3)_3$ (1 mol/L, 50 mL) was added dropwise to a solution of NaOH (6 mol/L, 25 mL) under vigorous stirring until the pH of the final solution was stabilized at 7. The resulting suspension was centrifuged at 4000 r/min, and the precipitate was washed using ultra-pure water (>18 MΩ/cm) and freeze-dried. The final product was ground to pass a 200-mesh sieve and stored at 4°C.

1.3. Adsorption experiments

Batch adsorption experiments were performed in two different systems: (Nowack et al., 2012) adsorption of PHF; (Hou et al., 2017) adsorption of PHF in the presence of different anions. In system 1, the adsorption kinetic experiment was first carried out at initial PHF concentration of 100 mg/L, and then the adsorption isotherm was measured using initial PHF concentrations of 10–500 mg/L. In addition, the effects of solution pH on the adsorption of PHF were further studied at a solution concentration of 100 mg/L and at pH ranging from 3 to 11. In system 2, PHF and the competing anions (phosphate, sulfate, or carbonate) were adsorbed simultaneously on Fh. The initial concentration of PHF was 50 mg/L (*i.e.*, 0.033 mmol/L), and the initial concentrations of the anions (phosphate, sulfate, or carbonate) were set to 0.033, 0.33, or 1.65 mmol/L (*i.e.*, the corresponding molar ratios of anions to PHF were 1, 10, or 50). The concentrations of anions were within the scope of those in natural water bodies (Presser and Ohlendorf, 1987; Froelich, 1988). As the experiments were conducted in sealed polypropylene bottles under acidic conditions, the trace amount of dissolved CO_2 was ignored.

All batch experiments were carried out by adding 0.05 g Fh with 20 mL of solutions containing different concentrations of PHF in the absence and presence of other anions, to 50 mL polypropylene bottles which were then vigorously shaken on an orbital shaker at 150 r/min for 24 hr at 25°C. All experiments were carried out at pH 5 in 1 mmol/L $NaNO_3$ solution unless otherwise stated. After the reactions reached equilibrium, the polypropylene bottles were centrifuged at 4000 r/min for 10 min to separate the reaction products. The concentration of PHF was determined using total organic carbon (TOC) measurements (Shimadzu TOC-VCPH analyzer, Shimadzu Scientific Instruments, Japan).

1.4. Zeta potential measurement and titration of surface sites

Zeta potential measurements of PHF (50 mg/L), Fh, and PHF-Fh (Fh after adsorption of 50 mg/L PHF) at different pH were carried out with a Malvern Zetasizer Nano-ZS (UK) using a refractive index of 2.2. 0.05 g of Fh or PHF-Fh powder was added to 20 mL of 1 mmol/L $NaNO_3$ solution. The pH of the suspensions was adjusted using HNO_3 and NaOH solutions. A solution of PHF was tested with the same procedure used for the suspension samples.

The surface sites of Fh and PHF-Fh were determined using the *in situ* Gran plot method, which is commonly used to determine the total surface site density of oxide minerals in contact with a solution (Tang et al., 2015). 0.2 g of Fh or PHF-Fh powder was added to 50 mL of 0.01 mol/L NaCl solution and measured against a blank control (50 mL of 0.01 mol/L NaCl solution). The resulting suspensions were stirred on a magnetic stirring apparatus for 12 hr. Afterwards, the solution pH was adjusted to 3 (0.1057 mol/L of HCl); and then back-titrated to 11 (0.1250 mol/L of NaOH). During the hydroxyl back-titration process, the added NaOH first reacted with the excess HCl added in the acid titration. After that, the added hydroxyl began to react with the hydroxyl groups on the surface of Fh; and the remainder contributed to the increase in the pH value of the system. The pH measurement was conducted with a pH-meter (PHS-3C, Shanghai LeiCi, China).

1.5. Characterization

X-ray diffraction (XRD) patterns of Fh were recorded using a Bruker D8 ADVANCE X-ray diffractometer (Karlsruhe, German), operating at 40 kV and 40 mA using CuKα radiation. The patterns were recorded over the 2θ range of 10–80° at a scanning speed of 1°/min. Nitrogen sorption–desorption isotherms at 77 K were determined by means of a NOVA 2200e Surface Area & Pore Size Analyzer from Quantachrome (Boynton Beach, Florida, USA), using samples that were previously degassed under vacuum at 50°C for 16 hr. The relative pressure (P/P_0) range of 0.05–0.35 was selected for the calculation of BET surface areas.

Atomic force microscope (AFM) images of the samples before and after the adsorption of PHF were captured using a commercial AFM (Bruker Multimode 8, America) equipped with a NanoScope V8 controller and ScanAsyst-Air SPM probes (cantilever spring constant 0.4 N/m). The samples for AFM imaging were dispersed in water under sonication, then the supernatants were dropped onto the surface of the fresh mica substrates and fully dried at room temperature before the measurement.

Transmission electron microscopy (TEM) was performed using a FEI Talos F200S (FEI Co., USA) microscope with the accelerating voltage of 200 kV. Samples for TEM imaging were prepared by a procedure similar to the samples for AFM imaging. The suspensions of samples were dropped onto the surface of a silicon nitride pane for further energy-dispersive X-ray spectroscopic (EDS) elemental (C, O, and Fe) mapping performed in scanning TEM mode.

Fourier-transform infrared (FT-IR) spectra of Fh before and after the adsorption of PHF were obtained using a Bruker VERTEX 70 spectrometer (Karlsruhe, Germany) and pressed KBr disks. The disks were prepared by pressing a mixture of powdered sample (0.9 mg) and KBr (80 mg). All spectra were recorded in the range of 4000–400 cm^{-1} with a resolution of 4 cm^{-1} and 64 scans.

2. Results and discussion

2.1. Characterization of Fh

The synthesized Fh showed two broad characteristic peaks at 2θ of ~34° and ~61° (Appendix A Fig. S1), confirming the formation of two-line Fh particles (Schwertmann and Cornell, 1991). BET analysis for the synthesized Fh indicated that it had a large specific surface area (309 m^2/g), consistent with the results reported by Schwertmann and Cornell (1991).

2.2. Adsorption kinetics and isotherm of PHF on Fh

Adsorption of PHF (100 mg/L) on Fh reached equilibrium after 24 hr (Appendix A Fig. S2), and therefore 24 hr was chosen as the equilibrium time for all the following adsorption experiments. The adsorption kinetic data were fitted to different adsorption models, including the pseudo first-order reaction model, the pseudo second-order reaction model, and the Elovich kinetic model (Appendix A Table S1). The pseudo second-order model gave the best fit, suggesting that the overall rate of adsorption is determined by the rate of the direct adsorption/desorption process, but not the intraparticle diffusion process (Plazinski et al., 2009).

The adsorption isotherm (Fig. 1a) showed a rapid increase of PHF uptake on Fh at low PHF concentrations, followed by a weak increase of adsorption at elevated PHF concentrations. The adsorption isotherm was fitted with Langmuir, Freundlich, Temkin, and Dubinin-Radushkevich (D-R) models to help understand the mechanism of the interaction between PHF and Fh. Generally, the Langmuir model assumes monolayer adsorption, which often occurs at a finite number of definite localized sites (Ma et al., 2016). The Freundlich model is an empirical model that can be applied to multilayer adsorption on heterogeneous surfaces (Foo and Hameed, 2010). The latter two models are primarily focused on the thermodynamic properties of the adsorption process. The Temkin model assumes that the adsorption heat decreases linearly with the adsorbate coverage (Foo and Hameed, 2010). The D-R model, nevertheless, is usually used to distinguish between physical and chemical adsorption, according to the mean free energy per molecule of adsorbate

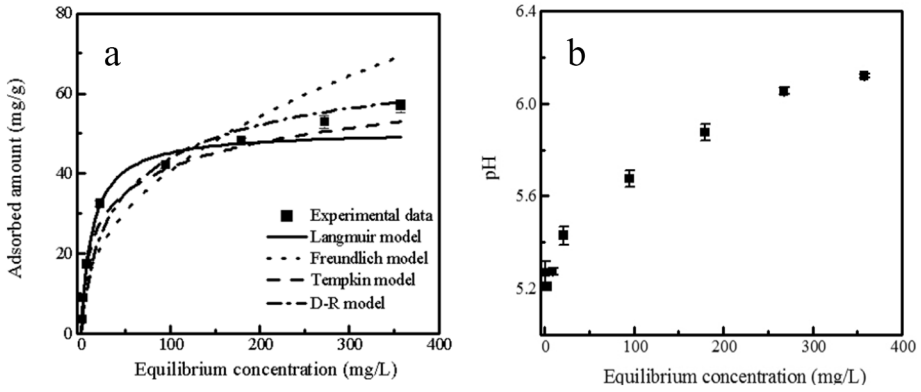

Fig. 1 – Adsorption isotherm for polyhydroxy fullerenes (PHF) on ferrihydrite (Fh) (a); the final solution pH as a function of equilibrium concentration (b).

(Foo and Hameed, 2010). The Temkin and D-R models fitted the experimental isotherm better, as indicated by the R^2 values (Appendix A Table S2). According to the fitted data from the D-R model, the maximum adsorption amount of PHF was calculated to be 67.1 mg/g and the mean free energy of PHF adsorption was 10.72 kJ/mol. As described in previous research, the adsorption should be considered a chemical interaction when the mean free energy is greater than 8 kJ/mol (Onyango et al., 2004; Foo and Hameed, 2010).

After the adsorption of PHF, the equilibrium solution pH increased rapidly (Fig. 1b), indicating the release of hydroxyl ions into the solution. The increase in solution pH is commonly observed in the adsorption of oxyanions (*e.g.*, phosphate, arsenate) by metal (oxyhydr)oxides, and a ligand exchange process is often proposed for the adsorption mechanism, *i.e.*, an exchange of the surface hydroxyl groups on metal (oxyhydr)oxides by oxyanions. Likewise, PHF might act similar to oxyanions and be adsorbed on Fh through a ligand exchange process. Indeed, previous investigations suggested that PHF existed as anionic forms in nature through the deprotonation of the surface hydroxyls (Zhang et al., 2010; Qu et al., 2012).

2.3. Effects of initial solution pH on the adsorption of PHF on Fh

PHF could be adsorbed on Fh over the pH range from 3 to 11 (Fig. 2a) and the adsorption amount of PHF decreased gradually with increasing pH. As the zeta potential of PHF was less than –15 mV over the entire pH range of our experiments (Fig. 3a), at pH greater than pH_{pzc} (8.5), specific interactions (*e.g.*, chemical adsorption), which can overcome the electrostatic repulsion, should exist between PHF and Fh; whereas at pH lower than 8.5, the adsorption of PHF on Fh can be attributed to electrostatic attractions, ligand exchange, and hydrogen-bond interactions (Antelo et al., 2005; Das et al., 2013). The decreased adsorption of PHF with increasing pH could be due to the change of Fh surface charge and the competitive effect of the hydroxyl anions. On one hand, as the surface charge of Fh reversed from positive (pH < 8.5) to negative (pH > 8.5) with increasing pH, the electrostatic interactions between PHF and Fh would become weaker. On the other hand, the hydroxyl anions, with high concentration at higher pH, could compete with PHF for the active binding sites on Fh, which should also have an adverse effect on the removal of PHF from solution (Otte et al., 2013; Liu et al., 2016).

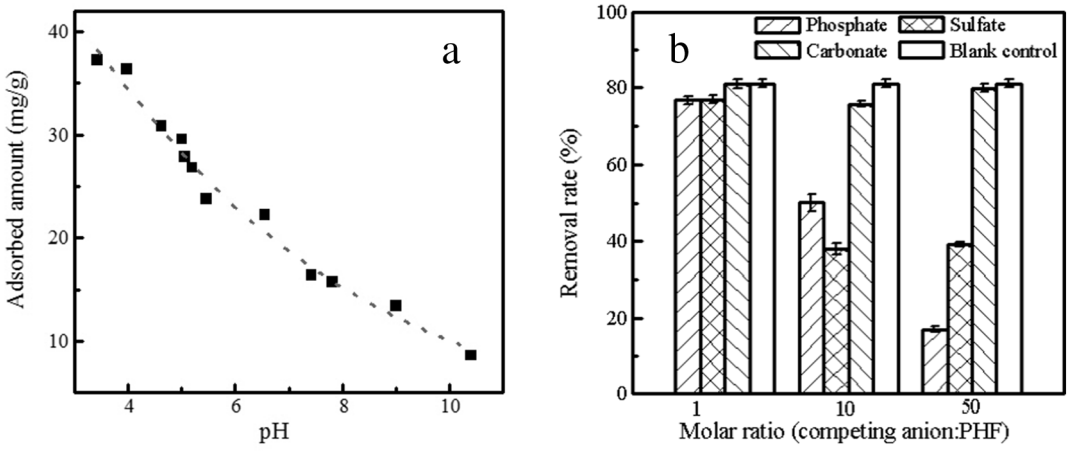

Fig. 2 – Effects of initial solution pH on PHF adsorption onto Fh (a); effects of competing anions on PHF adsorption onto Fh (b).

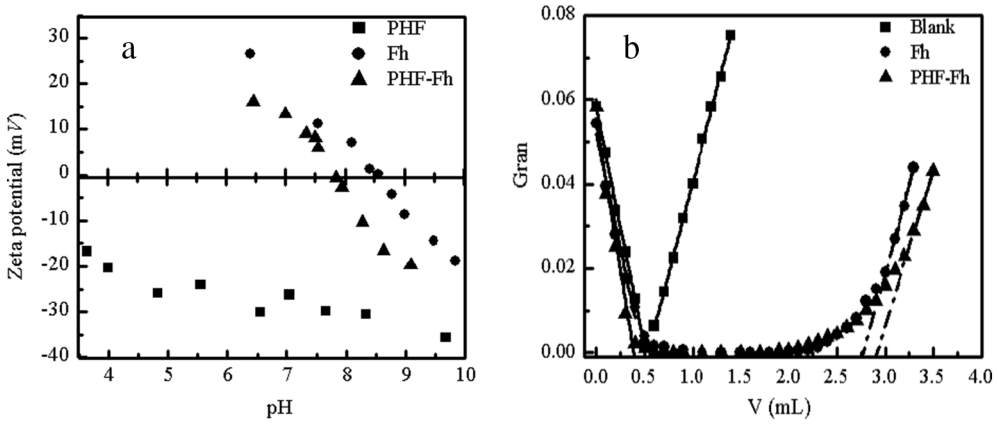

Fig. 3 – Zeta potential of PHF, Fh and PHF-Fh (a); Gran plots of Fh and PHF-Fh (b).

2.4. *Effects of co-existing oxyanions on the adsorption of PHF on Fh*

The mobility of PHF in the environment could be influenced by co-existing anions in natural aqueous systems. The obtained results demonstrated that at molar ratios of up to 50, carbonate had a negligible effect on the adsorption of PHF (Fig. 2b). Although phosphate and sulfate also had minor influences on PHF adsorption at low concentration (*i.e.*, at molar ratio of 1), they could drastically influence the adsorption of PHF on Fh as their concentration increased (at molar ratio from 10 to 50). The removal rate of PHF decreased to 50% in the presence of phosphate at a molar ratio of 10, and to 18% at molar ratio of 50. Only 40% of PHF was adsorbed in the presence of sulfate at molar ratios of 10 and 50. The competitive abilities of the co-existing anions could be attributed to the anion valence and their affinity to the binding surface sites (Su and Puls, 2001).

These results indicated that PHF could strongly interact with Fh; and the co-existing anions with comparable concentration had negligible effects on their adsorption. Only when the concentrations of phosphate and sulfate were greater than 10 mg/L could they significantly inhibit the adsorption of PHF. Still, the results of this work further implied that PHF might also compete with other groundwater pollutants.

2.5. *The surface zeta potential and site density of Fh*

The surface zeta potential of Fh (Fig. 3a) decreased after the adsorption of PHF. At the same time, the pH_{pzc} of Fh shifted from 8.5 to 8.0. During the adsorption process, the incoming

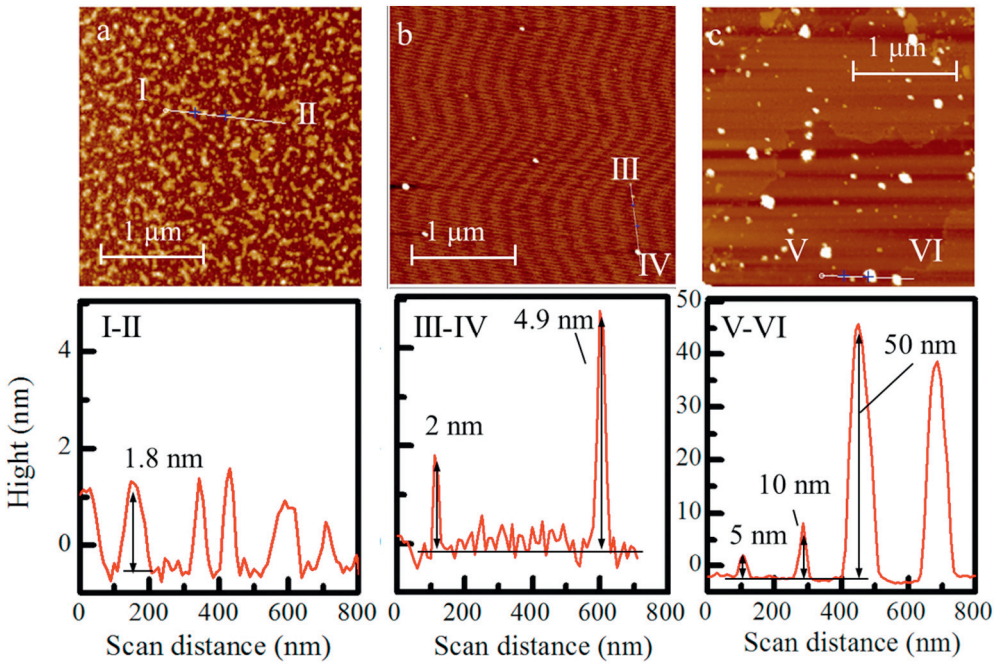

Fig. 4 – Atomic force microscopy (AFM) images of PHF (a), Fh (b), and PHF-Fh (c); the height images (underside) of the corresponding sections in AFM images.

PHF resulted in a more negative surface charge. Similar behavior was observed in the adsorption of oxyanions on iron (oxyhydr)oxides (Hiemstra and Riemsdijk, 1996). The surface site density of Fh was calculated using an *in situ* Gran plot (Fig. 3b), and the obtained value was 2.78 sites/nm^2, in line with literature results (Hiemstra et al., 2009) ranging from 2.5 to 9 sites/nm^2. Thus, Fh after the adsorption of PHF had a stronger buffering ability toward the hydroxyl in the solution, and its surface site density increased to 3.01 sites/nm^2.

The adsorbed PHF not only changed the surface electrostatic properties but also increased the number of proton active surface sites of Fh. Thus, one might expect that the adsorbed PHF could further affect the reactivity of Fh, *e.g.*, its interactions with other environmental chemicals. Our preliminary study further verified this speculation. The adsorption capacity of Fh toward Cd(II) (120 mg/L) increased by 167% and 629% after 20 and 50 mg/L of PHF loading, respectively (Appendix A Fig. S3). Thus, PHF in the environment could change the

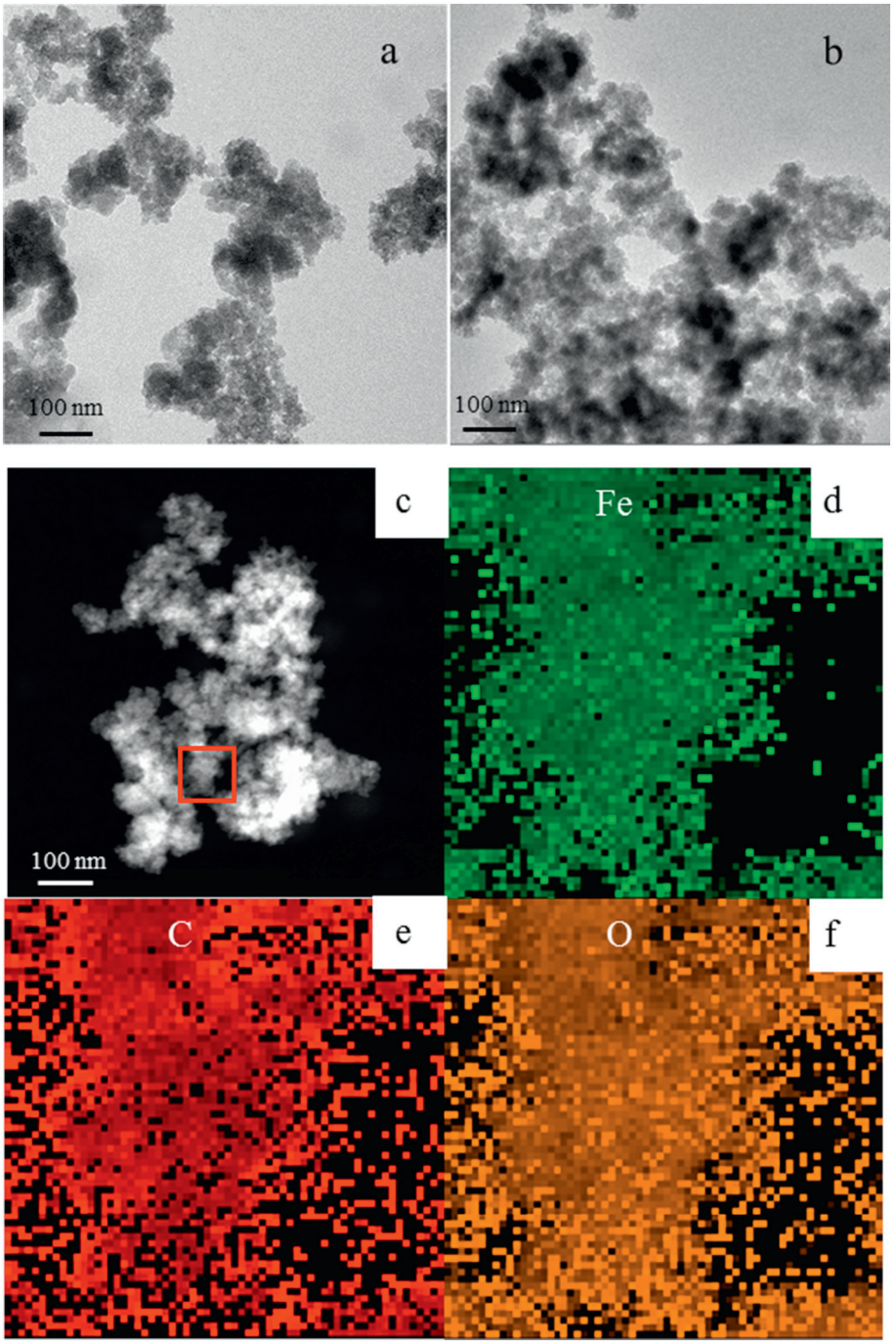

Fig. 5 – Transmission electron microscopy (TEM) images of Fh (a) and PHF-Fh (b); scanning TEM image of PHF-Fh (c) and the corresponding energy-dispersive X-ray spectroscopic (EDS) mappings showing Fe (d), C (e), and O (f) distributions in the selected area.

surface physicochemical properties of iron (oxyhydr)oxides (*e.g.*, Fh), which might further affect the immobilization of environmental contaminants such as heavy-metal cations.

2.6. The particle size and surface morphology of Fh

The PHF protrusions (Fig. 4) measured by AFM were amorphous aggregates, with a few spots on the mica plate. The average height of the protrusions was determined to be 1.8 nm, nearly the diameter of an individual PHF molecule. Being distinct from the PHF protrusions, the images of Fh and PHF-Fh were clearly observed as scattered spots in various examined views. Individual Fh particles were observed as spherical nanoparticles with the height of 1.8 nm and some small aggregates no taller than 5 nm. On the other hand, the PHF-Fh particles were higher than 5 nm and some aggregates were 50 nm high. Although adsorbed PHF could increase the particle size of Fh to some extent, the individual particle size of PHF-Fh was larger than the sum of the individual particle sizes of Fh and PHF, indicating aggregation of Fh due to the PHF loading, and the various sizes of aggregates also implied different degrees of aggregation.

Both the Fh and PHF-Fh were present as aggregates of nanoparticles smaller than 10 nm, as revealed by TEM imaging (Fig. 5). The spatial distributions of C, Fe, and O in the PHF-Fh aggregates detected by EDS mapping demonstrated that PHF and Fh were distributed rather evenly. Thus, we propose that PHF molecules act as bridges to link the adjacent Fh particles, causing significant aggregation of Fh particles. This phenomenon can also be explained by the decrease in the electrostatic repulsive forces between Fh particles due to the decrease of surface charge, as revealed by zeta potential measurements. The aggregation could significantly affect a variety of reactions of Fh, such as redox reactions, dissolution, and mineral transformation (Baalousha, 2009).

2.7. FT-IR characterization results

The FT-IR spectra of PHF, Fh, and Fh after the adsorption of different concentrations of PHF were collected, and the spectra of Fh samples before and after the adsorption were normalized for further analysis (Fig. 6). The assignments of the observed FT-IR bands were summarized (Appendix A Table S3). The PHF spectrum displayed relatively sharp bands at 1075 cm^{-1} for C–O stretching, at 1372 cm^{-1} for C–O–H asymmetry bend, at 1600 cm^{-1} for C=C stretching, and a shoulder peak at 1430 cm^{-1} for C–C vibration (Xing et al., 2004; Kokubo et al., 2011; Vaughan et al., 2012). The spectrum of Fh showed adsorption bands at 1493 and 1365 cm^{-1}, which were assigned to Fe–O and Fe–O–H bending modes, respectively (Towe and Bradley, 1967; Vaughan et al., 2012). With increasing amounts of adsorbed PHF, the bands of Fe–O (related to Fh) diminished, whereas the intensity of the shoulder band at 1430 cm^{-1}, due to C–C vibrations of PHF, gradually increased. In addition, a red shift of the C–O stretching band from 1075 cm^{-1} to 1062 cm^{-1} was observed after the adsorption. The red shift of C–O stretching and the decrease of Fe–O bending, in combination with the observed hydroxyl release during the batch adsorption experiment, revealed that the oxygen groups of PHF reacted with the surface sites of Fh, probably through a ligand exchange mechanism (Vermeer et al., 1998). In addition, the vibration band of nitrate at 1384 cm^{-1} indicated that nitrate could also be adsorbed on Fh; and its adsorption amount decreased (*i.e.*, absorption intensity decreased) as the loading amount of PHF increased. In this case, anion exchange with nitrate might also contribute to the adsorption of PHF on Fh. Hence, PHF in

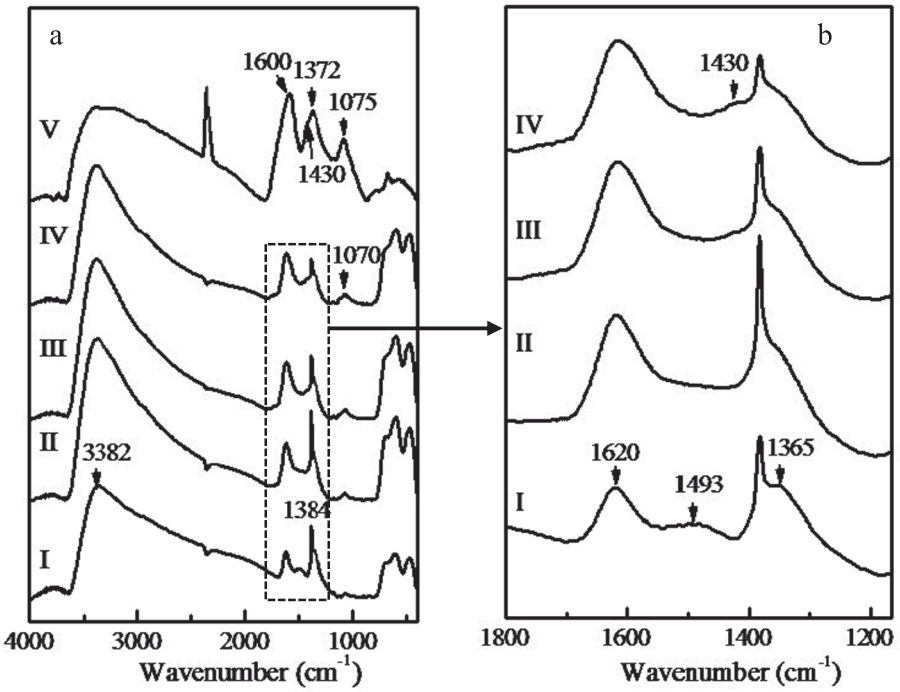

Fig. 6 – FTIR (Fourier-transform infrared) spectra of Fh (I), Fh after adsorbing PHF (100 mg/L (II), 200 mg/L (III), and 400 mg/L (IV)), and PHF (V). Panel b is the enlarged image of the square area as shown in panel a.

solution functioned similarly to oxyanions (*e.g.*, phosphate) and they could be immobilized through ligand exchange with the surface hydroxyl groups of Fh and through anion exchange with the surface adsorbed anions on Fh (*e.g.*, nitrate).

3. Conclusions

The present study provided fundamental data for gaining insight into the interactions between PHF and Fh. PHF were effectively adsorbed by Fh, and the equilibrium solution pH increased rapidly after the adsorption. As the initial solution pH increased from 3 to 11, the adsorption of PHF decreased significantly. Our results further indicated that PHF were adsorbed on Fh through the combined contribution of ligand exchange and anion exchange. In addition, the adsorbed PHF could trigger the aggregation of the Fh nanoparticles, as observed by AFM and TEM, by changing their surface physicochemical properties. Further investigation will be needed to elucidate the interaction between PHF and Fh over the longer term (*e.g.*, the effects of PHF on the transformation of Fh to more crystalized minerals; and the release of PHF during the transformation of Fh).

Acknowledgments

This is contribution No.IS-2420 from GIGCAS. This work was supported by the National Natural Science Foundation of China (No. 41572031), the National Program for Support of Top-notch Young Professionals, Guangdong Provincial Youth Top-notch Talent Support Program (No. 2014TQ01Z249), the Newton Advanced Fellowship Through the Royal Society in the United Kingdom (No. NA150190), and the National Key Research and Development Plan (No. 2016YFD0800700).

Appendix A. Supplementary data

Supplementary data to this article can be found online at http://dx.doi.org/10.1016/j.jes.2017.06.016.

REFERENCES

Antelo, J., Avena, M., Fiol, S., López, R., Arce, F., 2005. Effects of pH and ionic strength on the adsorption of phosphate and arsenate at the goethite-water interface. J. Colloid Interface Sci. 285, 476–486.

Baalousha, M., 2009. Aggregation and disaggregation of iron oxide nanoparticles: influence of particle concentration, pH and natural organic matter. Sci. Total Environ. 407, 2093–2101.

Chen, Q., Zhu, R., Zhu, Y., Liu, J., Zhu, L., Ma, L., Chen, M., 2016. Adsorption of polyhydroxy fullerene on polyethylenimine-modified montmorillonite. Appl. Clay Sci. 132, 412–418.

Das, S., Hendry, M., Essilfie, J., 2011. Effects of adsorbed arsenate on the rate of transformation of 2-line Ferrihydrite at pH 10. Environ. Sci. Technol. 45, 5557–5563.

Das, S., Hendry, M.J., Essilfie, J., 2013. Adsorption of selenate onto ferrihydrite, goethite, and lepidocrocite under neutral pH conditions. Appl. Geochem. 28, 185–193.

Foo, K.Y., Hameed, B.H., 2010. Insights into the modeling of adsorption isotherm systems. Chem. Eng. J. 156, 2–10.

Fortner, J., Solenthaler, C., Hughes, J., Puzrin, A., Plötze, M., 2012. Interactions of clay minerals and a layered double hydroxide with water stable, nano scale fullerene aggregates (nC60). Appl. Clay Sci. 55, 36–43.

Froelich, P.N., 1988. Kinetic control of dissolved phosphate in natural rivers and estuaries: a primer on the phosphate buffer mechanism. Limnol. Oceanogr. 33, 649–668.

Heimann, J., Morrow, L., Anderson, R.E., Barron, A.R., 2015. Understanding the relative binding ability of hydroxyfullerene to divalent and trivalent metals. Dalton Trans. 44, 4380–4388.

Hiemstra, T., Riemsdijk, V.W.H., 1996. A surface structural approach to ion adsorption: the charge distribution (CD) model. J. Colloid Interface Sci. 179, 488–508.

Hiemstra, T., Riemsdijk, W., Rossberg, A., Ulrich, K., 2009. A surface structural model for ferrihydrite II: adsorption of uranyl and carbonate. Geochim. Cosmochim. Acta 73, 4437–4451.

Hou, L., Fortner, J.D., Wang, X., Zhang, C., Wang, L., Chen, W., 2017. Complex interplay between formation routes and natural organic matter modification controls capabilities of C60 nanoparticles (nC60) to accumulate organic contaminants. J. Environ. Sci. 51, 315–323.

Indeglia, P.A., Krishna, V.B., Georgieva, A., Bonzongo, J.C.J., 2013. Mechanical transformation of fullerene (C60) to aqueous nano-C60 (aqu-nC60) in the presence and absence of light. J. Nanopart. Res. 15, 1–16.

Indeglia, P.A., Georgieva, A., Krishna, V.B., Bonzongo, J.C.J., 2014. Physicochemical characterization of fullerenol and fullerenol synthesis by-products prepared in alkaline media. J. Nanopart. Res. 16, 2599–2614.

Injac, R., Prijatelj, M., Strukelj, B., 2013. Fullerenol nanoparticles: toxicity and antioxidant activity. Oxidative Stress Nanotechnol. Methods Protoc. 1028, 75–100.

Jambor, J., Dutrizac, J., 1998. Occurrence and constitution of natural and synthetic ferrihydrite, a widespread iron oxyhydroxides. Chem. Rev. 98, 2549–2586.

Kokubo, K., Shirakawa, S., Kobayashi, N., Aoshima, H., Oshima, T., 2011. Facile and scalable synthesis of a highly hydroxylated water-soluble fullerenol as a single nanoparticle. Nano Res. 4, 204–215.

Kong, L., Tedrow, O.N., Chan, Y.F., Zepp, R.G., 2009. Light-initiated transformations of Fullerenol in aqueous media. Environ. Sci. Technol. 43, 9155–9160.

Kratschmer, W., Lamb, L.D., Fostiropoulos, K., Huffman, D.R., 1990. Solid C60: a new form of carbon. Nature 347, 354–358.

Liu, J., Zhu, R., Xu, T., Xu, Y., Ge, F., Xi, Y., Zhu, J., et al., 2016. Co-adsorption of phosphate and zinc(II) on the surface of ferrihydrite. Chemosphere 144, 1148–1155.

Ma, L., Zhu, J., Xi, Y., Zhu, R., He, H., Liang, X., Godwin, A.A., 2016. Adsorption of phenol, phosphate and Cd(II) by inorganic–organic montmorillonites: a comparative study of single and multiple solute. Colloids Surf. A 497, 63–71.

Mitsunobu, S., Muramatsu, C., Watanabe, K., Sakata, M., 2013. Behavior of antimony(V) during the transformation of Ferrihydrite and its environmental implications. Environ. Sci. Technol. 47, 9660–9667.

Murayama, H., Tomonoh, S., Alford, J.M., Karpuk, M.E., 2004. Fullerene production in tons and more: from science to industry. Fullerenes Nanotubes Carbon Nanostruct. 12, 1–9.

Nowack, B., Ranville, J.F., Diamond, S., Gallego-Urrea, J.A., Metcalfe, C., Rose, J., Klaine, S.J., 2012. Potential scenarios for nanomaterial release subsequent alteration in the environment. Environ. Toxicol. Chem. 31, 50–59.

Onyango, M.S., Kojima, Y., Aoyi, O., Bernardo, E.C., Matsuda, H., 2004. Adsorption equilibrium modeling and solution chemistry dependence of fluoride removal from water by trivalent-cation-exchanged zeolite F-9. J. Colloid Interface Sci. 279, 341–350.

Otte, K., Schmahl, W.W., Pentcheva, R., 2013. DFT+U study of arsenate adsorption on FeOOH surfaces: evidence for competing binding mechanisms. J. Phys. Chem. C 117, 15571–15582.

Plazinski, W., Rudzinski, W., Plazinska, A., 2009. Theoretical models of sorption kinetics including a surface reaction mechanism: a review. Adv Colloid Interface Sci. 152, 2–13.

Presser, T.S., Ohlendorf, H.M., 1987. Biogeochemical cycling of selenium in the San Joaquin valley, California, USA. Environ. Manag. 11, 805–821.

Qu, X., Alvarez, P.J.J., Li, Q., 2012. Impact of sunlight and humic acid on the deposition kinetics of aqueous fullerene nanoparticles (nC60). Environ. Sci. Technol. 46, 13455–13462.

Raven, K.P., Jain, A., Loeppert, R.H., 1998. Arsenite and arsenate adsorption on ferrihydrite: kinetics, equilibrium, and adsorption envelopes. Environ. Sci. Technol. 32, 344–349.

Schwertmann, U., Cornell, R., 1991. Iron Oxides in the Laboratory: Preparation and Characterization. Weinheim, Germany, VCH.

Schwertmann, U., Murad, E., 1983. Effects of pH on the formation of goethite and hematite from ferrihydrite. Clay Clay Miner. 31, 277–284.

Shi, R., Jia, Y., Wang, C., 2009. Competitive and cooperative adsorption of arsenate and citrate on goethite. J. Environ. Sci. 21, 106–112.

Su, C., Puls, R.W., 2001. Arsenate and arsenite removal by zerovalent iron: effects of phosphate, silicate, carbonate, borate, sulfate, chromate, molybdate, and nitrate, relative to chloride. Environ. Sci. Technol. 35, 4562–4568.

Swedlund, P., Webster, J., 1999. Adsorption and polymerisation of silicic acid on ferrihydrite, and its effect on arsenic adsorption. Water Res. 33, 3413–3422.

Tang, Y., Wang, J., Gao, N., 2010. Characteristics and model studies for fluoride and arsenic adsorption on goethite. J. Environ. Sci. 22, 1689–1694.

Tang, C., Zhu, J., Li, Z., Zhu, R., Zhou, Q., Wei, J., He, H., et al., 2015. Surface chemistry and reactivity of SiO_2 polymorphs: a comparative study on α-quartz and α-Cristobalite. Appl. Surf. Sci. 355, 1161–1167.

Towe, K.M., Bradley, W.F.J., 1967. Mineralogical constitution of colloidal "hydrous ferric oxides". J. Colloid Interface Sci. 24, 384–392.

Vaughan, G., Brydson, R., Brown, A., 2012. Characterisation of synthetic two-line ferrihydrite by electron energy loss spectroscopy. J. Phys. Conf. Ser. 371, 12079–12082.

Vermeer, A.W.P., Riemsdijk, W.H., Koopal, L.K., 1998. Adsorption of humic acid to mineral particles. 1. Specific and electrostatic interactions. Langmuir 14, 2810–2819.

Wang, X., Li, W., Richard, H., Liu, F., Parise, J.B., Feng, X., Sparks, D.L., 2013. Effect of ferrihydrite crystallite size on phosphate adsorption reactivity. Environ. Sci. Technol. 47, 10322–10331.

Wang, C., Zhang, H., Ruan, L., Chen, L., Li, H., Chang, X.L., Yang, S.T., 2016. Bioaccumulation of 13C-fullerenol nanomaterials in wheat. Environ. Sci. Nano 3, 799–805.

Xing, G., Zhang, J., Zhao, Y., Tang, J., Bo, Z., Gao, X., 2004. Influences of structural properties on stability of fullerenols. J. Phys. Chem. B. 108, 11473–11479.

Yamawaki, H., Iwai, N., 2006. Cytotoxicity of water-soluble fullerene in vascular endothelial cells. Am. J. Physiol. Cell Physiol. 290, 1495–1502.

Zhang, G., Liu, Y., Liang, D., Gan, L., Li, Y., 2010. Facile synthesis of isomerically pure fullerenols and formation of spherical aggregates from $C_{60}(OH)_8$. Angew. Chem. Int. Ed. 122, 5421–5423.

Zhang, F.L., Inganas, O., Zhou, Y., Vandewal, K., 2016. Development of polymer–fullerene solar cells. Natl. Sci. Rev. 3, 222–239.